



**HAL**  
open science

# Film-Forming Amines for the Corrosion Protection of Carbon Steels in Nuclear Power Plant Secondary Circuit Conditions: An Impedance Study

Jordan Baux, Nicolas Caussé, Sophie Delaunay, Jonathan Tireau, Marion Roy, Dominique You, Nadine Pébère

## ► To cite this version:

Jordan Baux, Nicolas Caussé, Sophie Delaunay, Jonathan Tireau, Marion Roy, et al.. Film-Forming Amines for the Corrosion Protection of Carbon Steels in Nuclear Power Plant Secondary Circuit Conditions: An Impedance Study. *Journal of The Electrochemical Society*, 2020, 167 (6), pp.061504. 10.1149/1945-7111/ab7d42 . hal-02880106

**HAL Id: hal-02880106**

**<https://hal.science/hal-02880106v1>**

Submitted on 24 Jun 2020

**HAL** is a multi-disciplinary open access archive for the deposit and dissemination of scientific research documents, whether they are published or not. The documents may come from teaching and research institutions in France or abroad, or from public or private research centers.

L'archive ouverte pluridisciplinaire **HAL**, est destinée au dépôt et à la diffusion de documents scientifiques de niveau recherche, publiés ou non, émanant des établissements d'enseignement et de recherche français ou étrangers, des laboratoires publics ou privés.






## Open Archive Toulouse Archive Ouverte (OATAO)

OATAO is an open access repository that collects the work of Toulouse researchers and makes it freely available over the web where possible

This is an author's version published in: <http://oatao.univ-toulouse.fr/26125>

**Official URL:** <https://doi.org/10.1149/1945-7111/ab7d42>

### To cite this version:

Baux, Jordan  and Caussé, Nicolas  and Delaunay, Sophie and Tireau, Jonathan and Roy, Marion and You, Dominique and Pébère, Nadine  *Film-Forming Amines for the Corrosion Protection of Carbon Steels in Nuclear Power Plant Secondary Circuit Conditions: An Impedance Study*. (2020) *Journal of The Electrochemical Society*, 167 (6). 061504. ISSN 1945-7111

Any correspondence concerning this service should be sent to the repository administrator: [tech-oatao@listes-diff.inp-toulouse.fr](mailto:tech-oatao@listes-diff.inp-toulouse.fr)

# Film-Forming Amines for the Corrosion Protection of Carbon Steels in Nuclear Power Plant Secondary Circuit Conditions: An Impedance Study

Jordan Baux,<sup>1,2</sup> Nicolas Caussé,<sup>1</sup> Sophie Delaunay,<sup>2</sup> Jonathan Tireau,<sup>2</sup> Marion Roy,<sup>3</sup>   
Dominique You,<sup>3</sup> and Nadine Pébère<sup>1,z</sup> 

<sup>1</sup>Université de Toulouse, CIRIMAT, UPS/INPT/CNRS ENSIACET, 31030 Toulouse Cedex 4, France

<sup>2</sup>EDF R&D/Chemistry and Corrosion Group, 77818 Moret sur Loing Cedex, France

<sup>3</sup>DEN Service d'Etude du Comportement des Radionucléides (SECR), CEA, Université Paris Saclay, F 91191 Gif sur Yvette, France

Octadecylamine (ODA) has been the subject of numerous investigations for the corrosion protection of carbon steels in nuclear pressurized water reactors (PWR). In the present work, electrochemical impedance spectroscopy was used to study and to compare the ODA behavior after different treatment temperatures (from 80 °C to 275 °C) representative of the secondary circuit of the PWR. The ODA films were characterized at room temperature. The impedance data analysis allowed the ODA film parameters (thickness and permittivity) to be obtained. The ODA film thickness was independent of the treatment conditions and was about 20 nm. At 120 °C and 220 °C, the presence of magnetite, formed during the treatment in the autoclave, strongly improved the corrosion protection afforded by the ODA films. An instantaneous inhibitive efficiency of 99.9% was assessed. At 275 °C, thermal degradation of the ODA molecules was shown.

[DOI: [10.1149/1945-7111/ab7d42](https://doi.org/10.1149/1945-7111/ab7d42)]

In the secondary circuit of nuclear pressurized water reactors (PWR), conservation conditions during shutdown and layup periods are a major issue to prevent corrosion phenomena that can affect feed water systems and steam generators. Conventional conservation programs are time consuming and, in some cases, constraining for operators due to the use of toxic additives.<sup>1</sup> An alternative method to those currently used to simplify metal surfaces conservation consists of their preservation with film forming amines (FFA), also known as fatty amines. FFA have been used for several decades to mitigate corrosion of materials in cooling water circuits.<sup>2-14</sup> FFA are known for their tendency to adsorb on metal or oxide surfaces by sharing the free electron pair of the amine nitrogen with the positively charged iron ions.<sup>15</sup> The aliphatic chain creates a hydrophobic physical barrier that prevent water, oxygen and other corrosive agents to reach the metal surface.<sup>3,16</sup> The protective film has been described by several authors as a monolayer.<sup>2,5,8</sup> The fatty amines are defined by the general formula  $R_1 [NH (R_2)]_n NH_2$ , where  $n$  is an integer between 0 and 7,  $R_1$  is an unbranched alkyl chain with 12 to 18 carbon atoms and  $R_2$  is a short chain alkyl group that usually contains 1 to 4 carbon atoms. Octadecylamine (ODA), one of the simplest FFA molecules ( $n = 0$ ,  $R_1 = C_{18}H_{37}$ ), has been the subject of numerous investigations both in thermal power plants<sup>6, 8, 11, 17-21</sup> and in nuclear power plants conditions.<sup>2, 3, 22-24</sup> Although steam generators have already been treated with FFA, their behavior is still not sufficiently well understood to define criteria ensuring optimal use.<sup>1</sup>

In a recent work,<sup>25</sup> an ODA film formed at 80 °C on a carbon steel surface has been characterized by using ex situ (optical observations, contact angle measurements and X ray photoelectron spectroscopy (XPS)) and in situ (electrochemical impedance spectroscopy (EIS)) measurements. The composition of the thin organic film has been determined from XPS and its physical characteristics (permittivity and thickness) obtained from EIS measurements. From the XPS analysis, the film thickness, in dry and vacuum conditions, was estimated between 2 and 10 nm. A film thickness of 16 nm was determined from the EIS data analysis, in good agreement with the XPS results. Thus, the impedance data analysis, by using both graphical methods and a power law model, allowed a methodology for the in situ characterization of organic thin films on conductive surface to be proposed.<sup>25</sup>

In order to move forward, the aim of the present work was to use the EIS technique to investigate the ODA behavior for the corrosion protection of a carbon steel in different conditions close to those encountered in the feed water systems of the PWR secondary circuit. To link the previous results, obtained on a bare carbon steel (rotating disk electrode (RDE)),<sup>25</sup> with data obtained in conditions representative of the PWR secondary circuit (pressurized equipment), a synthetic magnetite layer was first electrodeposited on the carbon steel surface, before the ODA film formation. Indeed, carbon steels and low alloy steels, which constitute the major part of the PWR secondary circuit, are covered by a thick layer of magnetite formed in normal operation.<sup>26,27</sup> The objective was to confirm the ODA ability to adsorb on corroded surfaces. Then, in a second step, the ODA films were formed in an autoclave at different temperatures (from 120 °C to 275 °C). Carbon steel samples were also exposed in the autoclave in the absence of ODA (reference samples). All the impedance measurements were afterwards performed in aerated condition and room temperature on the different samples to assess the presence or not of the ODA film. According to the methodology detailed in our previous paper,<sup>25</sup> the physical parameters of the ODA films were extracted from the impedance diagrams. In addition, the instantaneous corrosion inhibition efficiency was assessed.

## Experimental

**Materials.** P275 low carbon steel was supplied by EDF (France). Its composition is reported in Table I.

For  $T < 100$  °C, the working electrode was a rotating disk of 1 cm<sup>2</sup> surface area consisting of the cross section of a cylindrical rod (P275 carbon steel). The lateral part of the rod was covered with a heat shrinkable insulating sheath, leaving only the tip of the carbon steel in contact with the solution. The carbon steel surface was wet ground with silicon carbide (SiC) papers down to grade 4000, ultrasonically cleaned with ethanol, rinsed with deionized water and dried.

For  $T > 100$  °C, the experiments were performed in an autoclave. Carbon steel plates (20 mm × 30 mm × 3 mm) were used. The samples were wet ground with SiC papers down to grade 800 to comply with the initial surface state of carbon steel pipes in the nuclear industry. In the autoclave, a temperature probe allowed its precise monitoring (the temperature was controlled by a surrounding heater with an accuracy of ± 1 °C). A sampling hose was used to follow the chemistry of the solution inside the autoclave:

<sup>z</sup>E-mail: [nadine.pebere@toulouse-inp.fr](mailto:nadine.pebere@toulouse-inp.fr)



**Table I. Chemical composition (wt%) of the P275 carbon steel.**

Element	C	Si	Mn	Cr	Mo	Ni	Cu	Fe	
	0.16	0.4	0.5	1.5	0.3	0.08	0.5	0.3	Bal.

conductivity, pH and ODA concentration during the tests. A titanium mesh, attached to a rotating axis, carried three carbon steel plates. The rotation rate of the sample holder was maintained at 100 rpm.

ODA was in the form of ODACON<sup>®</sup>, a commercial emulsion ( $\approx 50 \text{ g L}^{-1}$  FFA) supplied by REICON<sup>TM</sup>.

**Electrochemical deposition of magnetite.** A magnetite layer was electrodeposited on the carbon steel during 30 min to ensure the formation of a thick layer, following the procedure described by Goujon et al.<sup>28</sup> A classical three electrode cell was used with a mercury sulfate electrode (MSE) in a saturated potassium sulfate solution as reference, a platinum grid as counter electrode and the RDE as working electrode. The rotation rate was fixed at 500 rpm. Figure 1 shows a top view and a cross section of the magnetite layer. After 30 min of deposition, its thickness is about  $40 \mu\text{m}$ . Through pores can be observed on the micrograph. The magnetite layer has been thoroughly characterized by Goujon et al.<sup>28</sup>

**ODA films formation.** At low temperature ( $T < 100 \text{ }^\circ\text{C}$ ), the ODA film formation on the electrodeposited magnetite was obtained with conditions similar to those used for the ODA film formation on the bare carbon steel.<sup>25</sup> The deposition conditions (ODA concentration, temperature, pH of the solution, immersion time and electrode rotation rate) are reported in Table II.

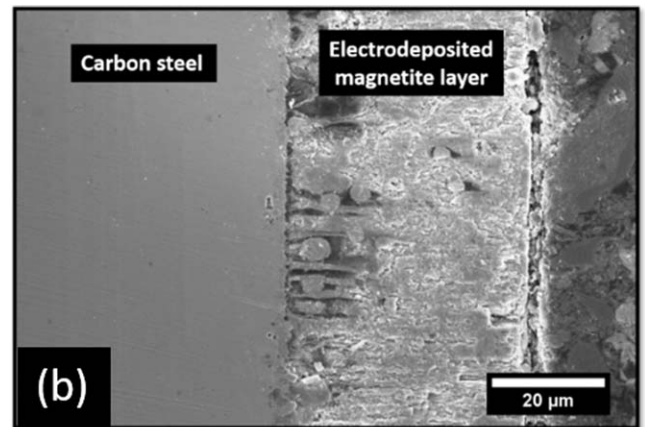
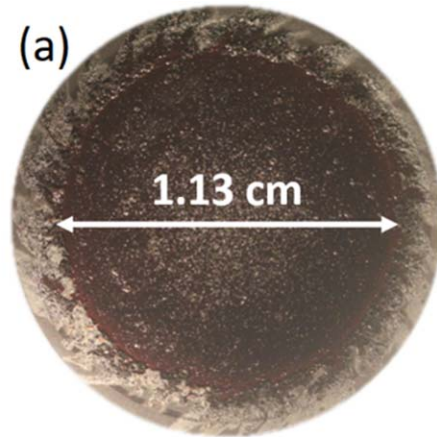
At higher temperatures ( $T > 100 \text{ }^\circ\text{C}$ ), the carbon steel plates were placed in the pressure equipment, the  $\text{pH}_{25 \text{ }^\circ\text{C}}$  of the solution was fixed between 9.6 and 9.8 with ammonia and ethanolamine. The electrolyte was deaerated with nitrogen bubbling before each experiment. Hydrazine was added ( $1 \text{ mg kg}^{-1}$ ) to ensure reducing conditions. For security reasons, the pressure equipment was not completely filled, and a steam phase was present above the liquid phase. Three test temperatures were chosen:  $120 \text{ }^\circ\text{C}$ ,  $220 \text{ }^\circ\text{C}$  and  $275 \text{ }^\circ\text{C}$ . These temperatures are representative of the water station, the entrance of the generator and the generator, respectively.<sup>1 3</sup> At  $120 \text{ }^\circ\text{C}$  and  $220 \text{ }^\circ\text{C}$ , the samples were dipped in the liquid phase. At  $275 \text{ }^\circ\text{C}$ , the samples were placed in the steam phase to reproduce the conditions of the upper part of the steam generators. The ODA concentration in the liquid phase was controlled to be close to  $2 \text{ mg kg}^{-1}$ , which is in the order of magnitude of the ODA concentration injected for the conservation of the circuit.<sup>1 3</sup> For  $220 \text{ }^\circ\text{C}$ , an additional experiment was carried out with a higher ODA concentration ( $25 \text{ mg kg}^{-1}$ ). For each temperature, carbon steel reference samples were prepared without ODA in similar conditions as described above.

**Surface characterizations.** For the surface characterizations, the electrodeposited magnetite and the samples from the autoclave were kept in contact with air for the shortest possible time.

Optical observations were performed with an Olympus PMG3 optical microscope. Scanning electron microscopy (SEM) images were obtained with a Zeiss Gemini Sigma in secondary electron mode. Energy dispersive X ray spectroscopy (EDX) analyses were

**Table II. Deposition parameters for the ODA film formation on the magnetite layer.**

ODA concentration	$100 \text{ mg kg}^{-1}$
Temperature	$80 \text{ }^\circ\text{C}$
Electrode rotation rate	500 rpm
$\text{pH}_{25 \text{ }^\circ\text{C}}$	10
Immersion time	30 min

**Figure 1.** Observations of the carbon steel surface (RDE) after the magnetite electrodeposition: (a) Top view (optical microscope) and (b) cross section (SEM).

performed at different locations on the carbon steel surface treated with ODA at  $120 \text{ }^\circ\text{C}$  to compare the chemical composition of the regions of interest.

The contact angles were measured at room temperature using a Krüss Mobile Surface Analyzer. The protocol consisted in depositing a deionized water drop of an accurate volume of  $1 \mu\text{l}$  on the sample surface and then measuring the static contact angle ( $\theta$ ) 60 s after the drop deposition. To assess the homogeneity of the surface properties, 20 measurements were performed on different locations on the samples surface.

**EIS measurements.** The impedance measurements were performed with a conventional three electrode cell with a mercury sulfate electrode (MSE) in a saturated potassium sulfate solution and a platinum grid, as reference electrode and counter electrode, respectively. The working electrode consisted of the carbon steel RDE or the carbon steel plate, depending on the temperature of the ODA films formation. In both cases, the surface area in contact with the electrolyte was  $1 \text{ cm}^2$ . The electrolytic solution was prepared from deionized water by adding  $10^{-3} \text{ M Na}_2\text{SO}_4$  (analytical grade). The choice of this medium was based upon its low electrical conductivity, close to that encountered in industrial water circuits, its low corrosiveness toward carbon steel and because it is an easily reproducible baseline solution. The pH was fixed at 10 with ammonia. A high pH value (around 10) is currently considered for secondary circuit conditioning to limit flow accelerated corrosion of carbon steels and to decrease the magnetite solubility.<sup>29 31</sup>

A Solartron 1286 electrochemical interface connected to a Solartron 1250 frequency response analyzer was used. EIS measurements were performed under potentiostatic regulation at the

corrosion potential ( $E_{corr}$ ) in the frequency range of 65 kHz to 1 MHz with 8 points per decade, using 15 mV<sub>rms</sub> sinusoidal voltage. The linearity was checked by varying the amplitude of the signal from 5 mV<sub>rms</sub> to 50 mV<sub>rms</sub>. At least two measurements were performed to ensure reproducibility. All the experiments were carried out at room temperature. Data modelling was carried out with a non commercial software developed at the LISE CNRS (Paris).

### EIS Data Analysis

When the presence of an ODA film was identified on the ODA treated samples, the impedance results were analyzed with a model to determine the thickness and the dielectric permittivity of the organic film, according to the recently developed methodology.<sup>25</sup> This methodology is briefly recalled below.

The impedance data are commonly analyzed by using electrical equivalent circuits, in which the capacitances are replaced by constant phase elements (CPE) to better describe the non ideal behavior of the interface. The CPE impedance, ( $Z_{CPE}$ ), is expressed in terms of model parameters  $\alpha$  and  $Q$  as:

$$Z_{CPE} = \frac{1}{(j\omega)^\alpha Q} \quad [1]$$

With  $\omega = 2\pi f$ . The  $\alpha$  and  $Q$  parameters can be graphically extracted.<sup>32</sup>

In the case of oxide films or organic coatings, the capacitance of the layers can be graphically extracted from the high frequency part of the impedance data, ( $Z(\omega)$ ), by using the complex capacitance representation:<sup>25,33,35</sup>

$$C(\omega) = \frac{1}{j\omega[Z(\omega) - R_e]} \quad [2]$$

Where  $C$  is the capacitance as a function of  $\omega = 2\pi f$  and  $R_e$  is the electrolyte resistance. The ODA film capacitance,  $C_f$ , was determined from the extrapolation at high frequency. Then, the dielectric layer thickness can be calculated using the following relationship:

$$\delta = \frac{\varepsilon\varepsilon_0}{C_f} \quad [3]$$

Where  $\varepsilon$ ,  $\varepsilon_0$  and  $\delta$ , represent the ODA dielectric permittivity, the vacuum permittivity and the ODA film thickness, respectively. For bulk ODA, a dielectric permittivity value of 2.7 was reported in the literature.<sup>36</sup>

Recently, different studies suggested that the origin of the CPE behavior observed with oxide films or organic coatings may be the consequence of a normal distribution of their resistivity along the film thickness according to the model developed by Hirschorn et al.<sup>37,38</sup> The resistivity  $\rho(\xi)$ , with  $\xi = \frac{x}{\delta}$ , is expressed (Eq. (4)) as a function of the layer thickness,  $\delta$ , the depth,  $x$ , in the layer, the boundary resistivity values  $\rho_0$  and  $\rho_\delta$  at the metal/film interface ( $x = 0$ ) and at the film/electrolyte interface ( $x = \delta$ ) and  $\gamma$  which is derived from the CPE parameter  $\alpha$  such as  $\alpha = \frac{(\gamma-1)}{\gamma}$ .

$$\frac{\rho(\xi)}{\rho_\delta} = \left( \frac{\rho_\delta}{\rho_0} + \left(1 - \frac{\rho_\delta}{\rho_0}\right)\xi^\gamma \right)^{-1} \quad [4]$$

The corresponding impedance can be determined using an integral expression:

$$Z_f(\omega) = \delta \int_1^0 \frac{1}{\frac{1}{\rho_0} + j\omega\varepsilon\varepsilon_0 + \left(\frac{1}{\rho_\delta} - \frac{1}{\rho_0}\right)\xi^\gamma} d\xi \quad [5]$$

Regression of EIS data with the power law model allows the extraction of physical parameters related to the film such as

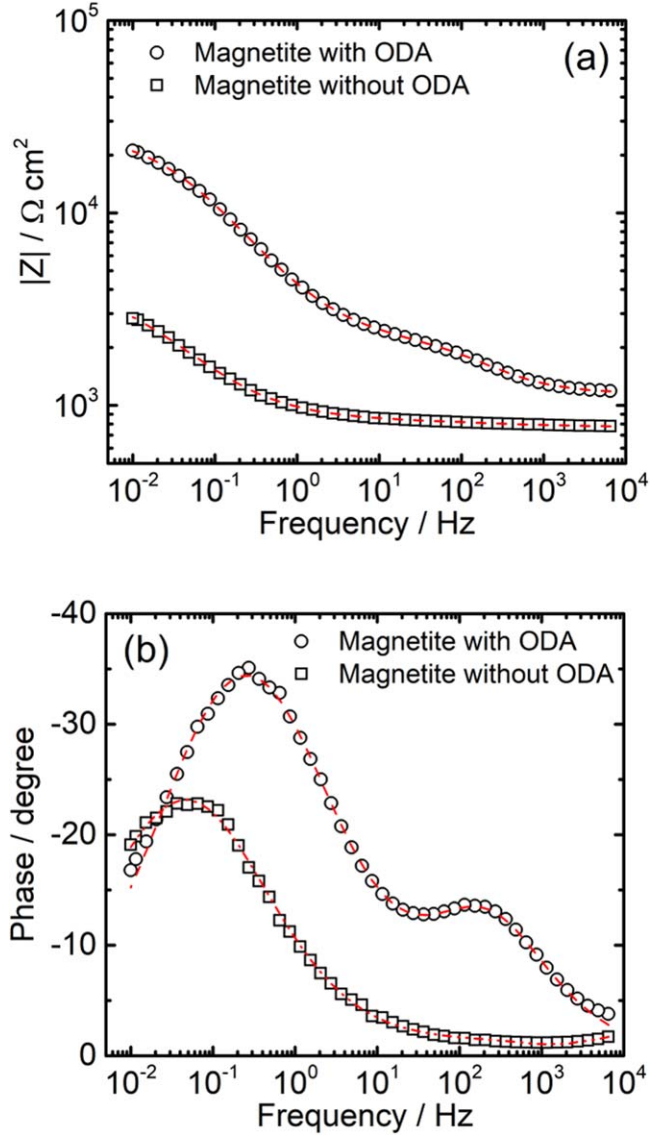


**Figure 2.** Electrochemical impedance diagrams for the carbon steel covered by the magnetite with ODA treatment (100 mg kg<sup>-1</sup>, 80 °C; 30 min; pH<sub>25</sub> °C 10,  $\Omega$  500 rpm) and without ODA. The diagrams are obtained after 2 h of immersion in the 10<sup>-3</sup> M Na<sub>2</sub>SO<sub>4</sub> solution. (a) Impedance modulus and (b) phase angle. The dotted lines are the fitted curves with the equivalent circuit shown in Fig. 10.

permittivity, thickness and resistivity values at the interfaces. In the present work, the ODA dielectric permittivity value obtained from the regression will be compared to that reported in the literature.<sup>36</sup>

### Results and Discussion

First, the ODA film formed on the magnetite layer (henceforth called ODA treated magnetite) is characterized by EIS. Then, the influence of the treatment temperature on the ODA films formation is discussed. In a third part, the impedance data are analyzed with the power law model in order to extract the physical parameters of the ODA films formed at different temperatures. Finally, the instantaneous corrosion inhibition efficiency is assessed from the impedance data obtained at the corrosion potential, with and without ODA.

**ODA treated magnetite.** The impedance spectra, in Bode coordinates, obtained for the magnetite layer and for the ODA treated magnetite after 2 h of immersion in the Na<sub>2</sub>SO<sub>4</sub> solution are

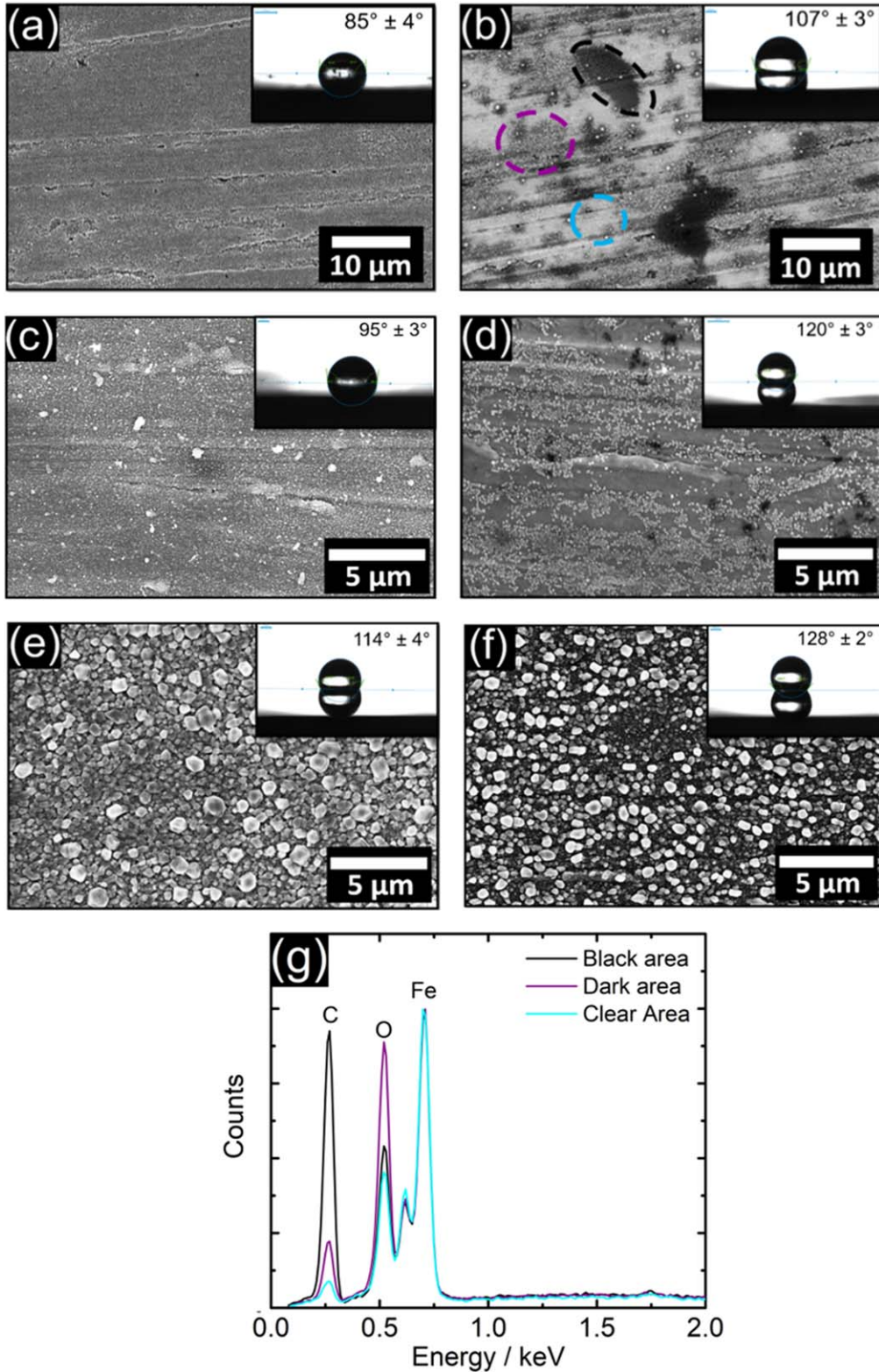


**Figure 3.** SEM micrographs of the carbon steel samples after the treatments in the autoclave. (a) 168 h at 120 °C without ODA ( $2\ \text{mg kg}^{-1}$ ), (b) 168 h at 120 °C with ODA ( $2\ \text{mg kg}^{-1}$ ), (c) 168 h at 220 °C without ODA, (d) 168 h at 220 °C with ODA ( $2\ \text{mg kg}^{-1}$ ), (e) 2 h at 275 °C in the steam phase without ODA, (f) 2 h at 275 °C in the steam phase with ODA ( $2\ \text{mg kg}^{-1}$  in the liquid phase) and (g) EDX spectra (normalized from the Fe peak) corresponding to different areas on the treated ODA carbon steel at 120 °C during 168 h (Fig. 3b).

presented in Fig. 2. For the magnetite layer, the impedance diagram is characterized by a single time constant related to the electrochemical behavior of the carbon steel/magnetite/electrolyte interface. After the ODA treatment, an additional time constant appears

at high frequency (between  $10^4$ – $10^5$  Hz), attributed to the presence of the ODA film.<sup>25</sup> Without ODA, the value of the impedance modulus at low frequency is about  $3200\ \Omega\ \text{cm}^2$ , close to that obtained for the bare carbon steel (mechanically polished) in the same conditions.<sup>25</sup>



This means that the thick electrodeposited magnetite layer does not strongly influence the electrochemical behavior of the interface. This could be attributed both to the porous structure of the magnetite, as observed in Fig. 1, and to its good conductive properties.<sup>39</sup> For the ODA treated magnetite, the impedance modulus at low frequency increases about one decade ( $24600 \Omega \text{ cm}^2$ ) which is, again, similar to the result previously obtained with ODA on the bare carbon steel.<sup>25</sup> These results underline that the ODA film has roughly the same signature on the impedance diagrams when adsorbed on the bare carbon steel or on the electrodeposited magnetite. These impedance data will be further analysed and the results will be discussed by comparison with those obtained after the treatments in the autoclave at temperatures higher than  $100^\circ\text{C}$ .

#### Carbon steel treated with ODA in the autoclave at $T > 100^\circ\text{C}$ .

**Surface observations and contact angle measurements.** SEM images of the surface morphology of the carbon steel samples treated at  $120^\circ\text{C}$ ,  $220^\circ\text{C}$  and  $275^\circ\text{C}$  in the autoclave, with and without ODA, are shown in Fig. 3. The formation of a magnetite layer is observed for all the coupons. The size of the magnetite crystallites increases when the treatment temperature increases, particularly for the samples treated at  $275^\circ\text{C}$  in the steam phase (Figs. 3e and 3f). In that case, the dissolution of the magnetite was limited in the steam and it accumulated on the samples surface. In the presence of ODA, dark areas are visible on the samples treated at  $120^\circ\text{C}$  and  $220^\circ\text{C}$  (Figs. 3b and 3d). Their composition was qualitatively analyzed by EDX for the sample treated at  $120^\circ\text{C}$  (Fig. 3g). A significant enrichment in carbon is observed which could be attributed to the presence of ODA clusters. Such clusters have already been observed for the bare carbon steel treated at  $80^\circ\text{C}$  with a higher ODA concentration ( $100 \text{ mg kg}^{-1}$ ).<sup>25</sup>

Contact angle measurements for the ODA treated samples at  $120^\circ\text{C}$  (Fig. 3b) and  $220^\circ\text{C}$  (Fig. 3d) highlight a change in the surface hydrophobicity by comparison with the non treated samples (Figs. 3a and 3c, respectively). The contact angles increase by around  $22^\circ$  and  $25^\circ$  for the ODA treated carbon steel at  $120^\circ\text{C}$  and  $220^\circ\text{C}$ , respectively, compared to the reference samples. This difference would be linked to the ODA adsorption on the surface. For the samples exposed at  $275^\circ\text{C}$  in the steam phase (Figs. 3e and 3f), the surface roughness, due to the formation of larger magnetite crystallites, could be at the origin of the increase of the contact angle, both with and without ODA. In that case, the contact angle measurement cannot be used to verify the ODA adsorption. As it will be shown further, there was no ODA film on the surface at this temperature.

**ODA film formation: influence of the deposition conditions.** The impedance diagram, in Bode coordinates, for the carbon steel treated in the autoclave with ODA ( $2 \text{ mg kg}^{-1}$ ) during 168 h at  $120^\circ\text{C}$  and after 2 h of immersion in the  $10^{-3} \text{ M Na}_2\text{SO}_4$  solution is presented in Fig. 4. The diagram is compared with that obtained for a reference sample (same conditions without ODA). The impedance modulus (Fig. 4a) at  $10^{-3} \text{ Hz}$  shows a significant increase after the ODA treatment (more than two decades) compared to the reference sample. In addition, the phase angle (Fig. 4b) reveals a very well defined time constant in the high frequency range, which is not visible on the reference sample, and related to the ODA film formation on the sample. Thus, the ODA is able to form a film on the carbon steel surface at  $120^\circ\text{C}$  in the representative thermochemical conditions of the secondary circuit. The significant increase of the impedance modulus after the ODA treatment could be due to the deposition condition (temperature and treatment time in the autoclave) and could also reveal a synergistic effect between the magnetite layer formation and the ODA adsorption.

Figure 5 shows the impedance diagrams of the carbon steel samples after the treatment in the autoclave at  $220^\circ\text{C}$ , with ODA ( $2 \text{ mg kg}^{-1}$  and 168 h of immersion (Figs. 5a and 5b) and  $25 \text{ mg kg}^{-1}$  and 2 h of immersion (Figs. 5c and 5d) and without ODA. With  $2 \text{ mg kg}^{-1}$  of ODA, the impedance diagram for the

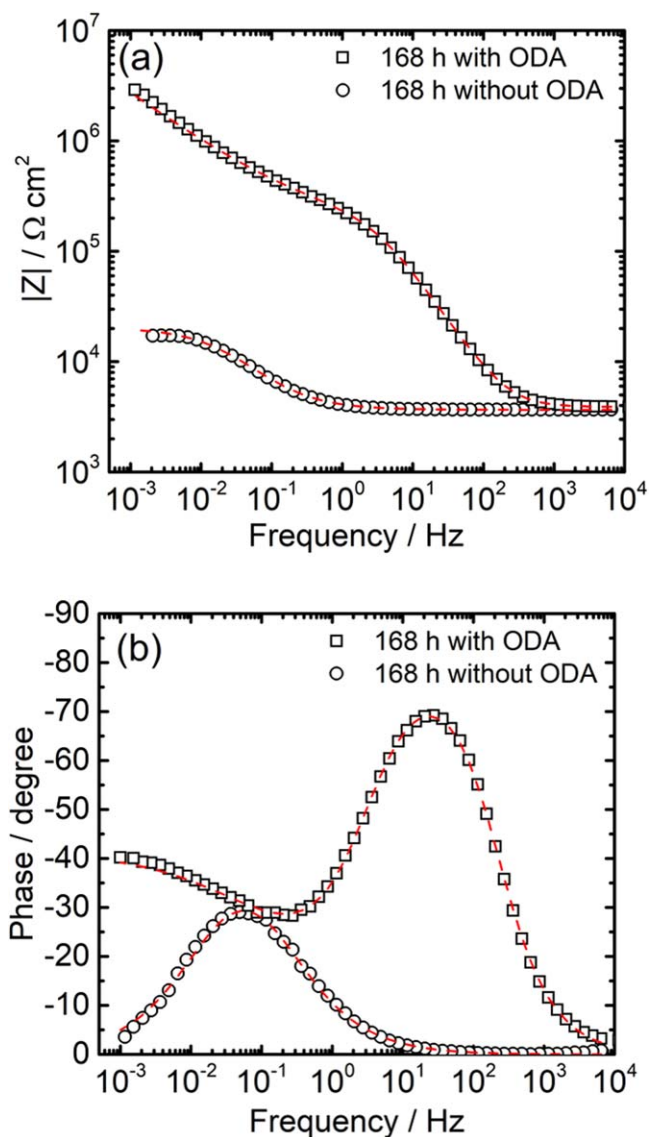


**Figure 4.** Electrochemical impedance diagrams for the carbon steel samples treated at  $120^\circ\text{C}$  during 168 h with ODA ( $2 \text{ mg kg}^{-1}$ ) and without ODA. The diagrams are obtained after 2 h of immersion in the  $10^{-3} \text{ M Na}_2\text{SO}_4$  solution. (a) Impedance modulus and (b) phase angle. The dotted lines are the fitted curves with the equivalent circuit shown in Fig. 10.

ODA treated sample (Figs. 5a and 5b) is relatively similar to that of the sample without ODA. This was unexpected because the contact angle measurements pointed out a more hydrophobic surface after the ODA treatment. Moreover, the SEM images suggested the presence of the organic molecules on the surface (dark areas in Fig. 3d). The impedance results indicate that the ODA molecules did not homogeneously cover the electrode surface, leaving film free areas without protection.

To check if it was possible to form an ODA film at  $220^\circ\text{C}$ , carbon steel coupons were treated in similar conditions with a higher ODA concentration ( $25 \text{ mg kg}^{-1}$ ). The impedance diagrams are displayed in Figs. 5c and 5d. It can be seen that after 2 h of treatment, the impedance modulus at  $10^{-3} \text{ Hz}$  (Fig. 5c) increases about 2 decades, similarly to what was observed after the treatment at  $120^\circ\text{C}$ , and a time constant, characteristic of the presence of the ODA film, is visible on the phase angle (Fig. 5d). Thus, the comparison of the EIS results for the samples treated with  $2 \text{ mg kg}^{-1}$  of ODA at  $120^\circ\text{C}$  (Fig. 4) and at  $220^\circ\text{C}$  (Figs. 5a and 5b) emphasizes the important role played by the temperature. To explain these results, the most likely hypothesis would be the

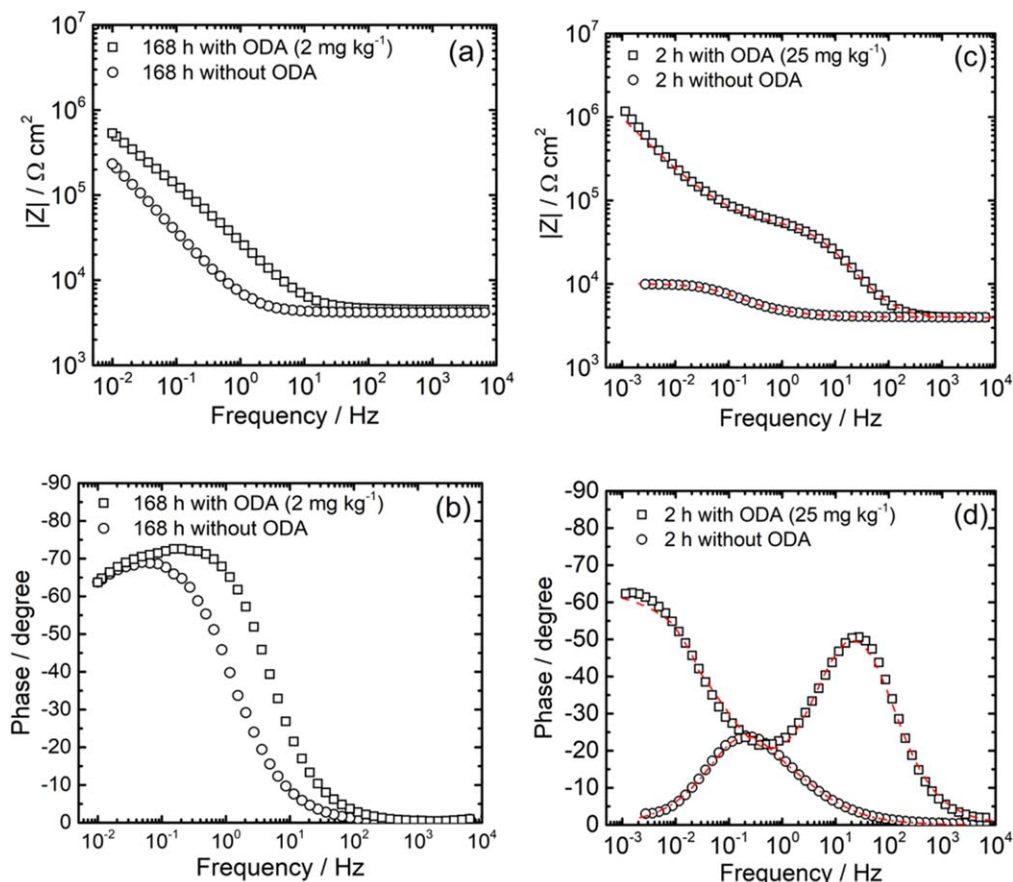


**Figure 5.** Electrochemical impedance diagrams for the carbon steel samples treated: (a), (b) at 220 °C during 168 h with ODA ( $2 \text{ mg kg}^{-1}$ ) and without ODA and (c), (d) at 220 °C during 2 h with ODA ( $25 \text{ mg kg}^{-1}$ ) and without ODA. The diagrams are obtained after 2 h of immersion in the  $10^{-3} \text{ M Na}_2\text{SO}_4$  solution. (a), (c) Impedance modulus and (b), (d) phase angle. The dotted lines are the fitted curves with the equivalent circuit shown in Fig. 10.

thermal degradation of the ODA at 220 °C and for long immersion times, as set out further.

Figure 6 compares the impedance diagrams obtained for the carbon steel treated at 275 °C after 2 h and 24 h in the presence of ODA ( $2 \text{ mg kg}^{-1}$ ) and after 2 h without ODA. The impedance modulus at low frequency is higher after 2 h of treatment with ODA ( $4 \times 10^6 \Omega \text{ cm}^2$ ) compared to the reference sample ( $2 \times 10^5 \Omega \text{ cm}^2$ ). However, the time constant characteristic of the film is hardly discernible (Fig. 6b). After 24 h of treatment, the impedance modulus decreases and the phase angle reveals a single time constant, indicating that the film effect disappeared after 24 h at 275 °C. The thermal degradation of the ODA molecules at 275 °C could explain this result.

To confirm this hypothesis, the ODA concentration in the liquid phase at 275 °C was determined as a function of time. The variation of the ODA concentration with time is reported in Fig. 7. It can be seen that the ODA concentration rapidly decreases. About 80 wt% of the initial concentration disappear during the first 6 h. After 24 h, the ODA concentration is almost zero. Thus, the absence of the ODA film response on the impedance spectra after 24 h of treatment (Fig. 6) and the rapid decrease of the ODA concentration in the liquid phase during the same period (Fig. 7) confirmed the thermal degradation of the ODA at 275 °C. The ODA degradation might also take place at 220 °C, which would explain the absence of the film after 168 h of treatment with  $2 \text{ mg kg}^{-1}$  ODA (Figs. 5a and 5b).

**EIS analysis. High frequency part: physical description of the ODA films.** The ODA films formed on the steel samples at different temperatures were characterized by analyzing the high frequency domain (10 Hz to 10 kHz) of the impedance diagrams. A focus was made on the determination of the ODA films thickness and on the

resistivity profiles obtained from the power law model. Due to the absence of a high frequency time constant on the impedance diagrams for the samples treated with ODA ( $2 \text{ mg kg}^{-1}$ ) during 168 h at 220 °C and during 2 h at 275 °C, the corresponding impedance results were not considered in the following.

The complex capacitance plots corresponding to the impedance diagrams with ODA presented in Figs. 2, 4 and 5c and 5d are displayed in Fig. 8, as well as the fitted curves with the power law model (Eq. 5). The regressed parameters are reported in Table III. For comparison, the values obtained for the ODA treated carbon steel<sup>25</sup> are added in Table III. It is interesting to note that in all cases, the ODA permittivity value extracted from the power law model is equal to 2.8 which is very close to the permittivity value found in the literature for bulk ODA ( $\epsilon = 2.7$ ).<sup>36</sup>

First, the result for the ODA treated magnetite is shown in Fig. 8a. The film thickness,  $\delta$ , calculated from Eq. 3 with  $C_f = 1.22 \times 10^{-7} \text{ F cm}^{-2}$  (graphically determined film capacitance) is identical to the extracted value with the power law model and is equal to 20 nm. This result is roughly consistent with that obtained on the carbon steel treated with ODA in the same deposition conditions.<sup>25</sup> The in depth resistivity profile of the ODA layer formed on the electro deposited magnetite was calculated from Eq. 4 and reported line (a) in Fig. 9. The profile is similar to that obtained on the treated carbon steel.<sup>25</sup> From Figs. 2, 8a and 9, it can be concluded that the ODA film formed on two different substrates (electrodeposited magnetite and carbon steel), in the same deposition conditions (treatment with  $100 \text{ mg kg}^{-1}$  ODA during 30 min at 80 °C), have the same physical characteristics.

The complex capacitance plot of the ODA treated carbon steel at 120 °C during 168 h with  $2 \text{ mg kg}^{-1}$  ODA is shown in Fig. 8b. The ODA film thickness, calculated from the film capacitance



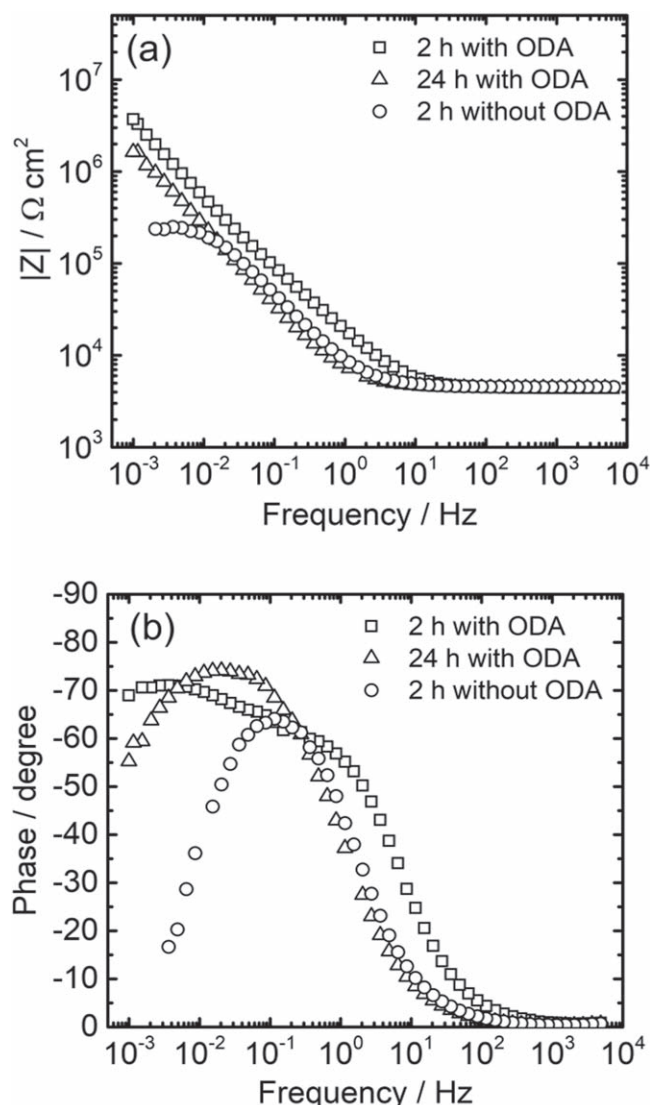


**Figure 6.** Electrochemical impedance diagrams for the carbon steel samples treated at 275 °C in the steam phase during 2 h and 24 h with ODA (2 mg kg<sup>-1</sup> in the liquid phase) and without ODA during 2 h. The diagrams are obtained after 2 h of immersion in the 10<sup>-3</sup> M Na<sub>2</sub>SO<sub>4</sub> solution. (a) Impedance modulus and (b) phase angle.

( $C_f = 1.42 \times 10^{-7} \text{ F cm}^{-2}$ ) and from the regression with the power law model, is equal to 18 nm. This value is relatively similar to that obtained after the treatment with 100 mg kg<sup>-1</sup> ODA at 80 °C during 30 min on the bare carbon steel (16 nm<sup>25</sup>) and on the magnetite (20 nm). Thus, it appears that the deposition conditions have little influence on the ODA film thickness.

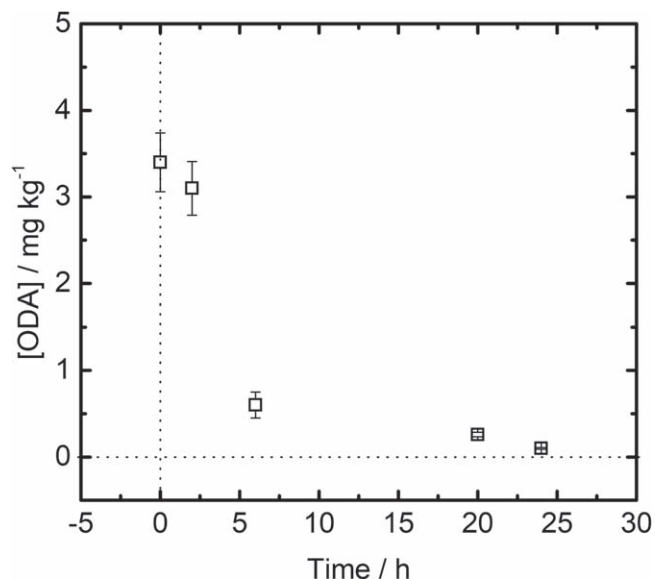


**Figure 7.** ODA concentration in the liquid phase at 275 °C as a function of time.

However, the in depth resistivity profile (line (b) in Fig. 9) is different from those obtained at low temperature. In this case, a high resistivity plateau ( $\rho_0 = 10^{12} \Omega \text{ cm}$ ) is observed over about half the ODA film thickness (approximately 10 nm), which is in agreement with the significant increase of the impedance modulus at low frequency after the ODA treatment. The physical origin of this high resistivity plateau is not yet understood. One hypothesis could be the incorporation of the ODA molecules in the magnetite layer formed during the treatment at 120 °C, which would lead to the formation of a compact mixed ODA/magnetite layer. This hypothesis is in agreement with previous studies.<sup>5,7</sup> It may be noted here that the high resistivity plateau was not observed on the ODA treated magnetite probably because the magnetite layer and the ODA film were deposited consecutively.

Finally, for the film formed during 2 h at 220 °C with 25 mg kg<sup>-1</sup> ODA, the film thickness,  $\delta$ , determined both graphically (Fig. 8c) and by regression with the power law model is equal to 15 nm, which is close to the ODA films thickness already obtained for the different treatment conditions. For this system, a slight deviation is visible at high frequency between the experimental and the regressed data ( $\chi^2 = 0.77$ ). In line (c) in Fig. 9, the resistivity profile highlights a high resistivity plateau ( $10^{11} \Omega \text{ cm}$ ) over about 4 nm thick. The lower resistivity value and the narrower plateau obtained after 2 h at 220 °C with 25 mg kg<sup>-1</sup> ODA compared with 168 h at 120 °C with 2 mg kg<sup>-1</sup> ODA might be linked to the influence of the treatment time.

*Low frequency part: corrosion inhibition efficiency.* In the absence of ODA, the impedance spectra obtained for the carbon

**Table III.** Regressed parameter values obtained with the power-law model for the ODA layers formed for different treatment conditions (temperature and concentration) on the carbon steel.

	Treated carbon steel at 80 °C, [ODA] 100 mg kg <sup>-1</sup> , 30 min Taken from Ref. 25	Treated magnetite layer at 80 °C, [ODA] 100 mg kg <sup>-1</sup> , 30 min	Treated carbon steel at 120 °C, [ODA] 2 mg kg <sup>-1</sup> , 168 h	Treated carbon steel at 220 °C, [ODA] 25 mg.kg <sup>-1</sup> , 2 h
$\delta/\text{nm}$	16	20	18	15
$\alpha$	0.78	0.67	0.95	0.89
$\epsilon$	2.8	2.8	2.8	2.8
$\rho_0 / \Omega \text{ cm}$	$1 \times 10^{10}$	$1 \times 10^{10}$	$9 \times 10^{11}$	$9 \times 10^{10}$
$\rho_\delta / \Omega \text{ cm}$	$1.6 \times 10^6$	$1 \times 10^7$	$8 \times 10^7$	$1 \times 10^6$
$\chi^2$	0.32	0.24	0.18	0.77

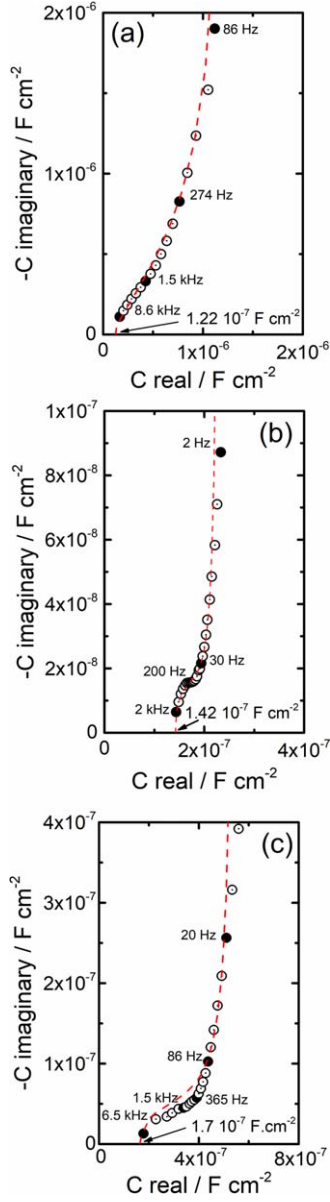


**Figure 8.** Complex capacitance plots corresponding to the EIS spectra presented in: (a) Fig. 2, (b) Fig. 4 and (c) Figs. 5c and 5d. The dotted lines are the fitted curves with the power law model (Eq. 5).

steel samples were characterized by a single time constant (Figs. 2, 4 and 5c and 5d). This time constant, between  $10^{-1}$  and  $10^{-2}$  Hz (or  $10^{-3}$  Hz), can be attributed to the processes occurring at the carbon steel/electrolyte interface. The presence of magnetite, which has a high electrical conductivity, has very little influence on the impedance response.<sup>39</sup> On the other hand, the ODA films are assumed to be strongly adsorbed on the samples surface as suggested by the high resistivity at the metal/film interface (Fig. 9). Nevertheless, the ODA films were very thin (about 20 nm) and the corrosion process would occur on a reduced surface area. As a first

approximation, we can consider that the second time constant observed on the impedance diagrams for the ODA treated samples is due to the charge transfer process at the bottom of the through pores of the ODA layer, at the magnetite/electrolyte interface. Without ODA, the parameters associated with the single time constant were determined with a simple R//CPE circuit ( $R_t$ ,  $Q_{dl}$  and  $\alpha_{dl}$ ). For the ODA treated samples, the parameters were determined by using the equivalent circuit shown in Fig. 10. The dotted lines in Figs. 2, 4 and 5c and 5d are the fitted curves with the equivalent circuit. As it can be seen, the experimental data are in perfect agreement with the fitted data. The fitted parameter values ( $R_t$ ,  $Q_{dl}$  and  $\alpha_{dl}$ ) are reported in Tables IV, V and VI.

From the CPE parameters ( $\alpha_{dl}$  and  $Q_{dl}$ ), the double layer capacitance ( $C_{dl}$ ) values were calculated by using the Brug formula:<sup>40</sup>

$$C_{dl} = Q_{dl} \frac{1}{\alpha} \left( \frac{1}{R_e} + \frac{1}{R_t} \right)^{(\alpha-1)/\alpha} \quad [6]$$

The  $R_t$  values were used to calculate the instantaneous inhibitive efficiency (IE) according to the following equation:

$$IE\% = \frac{R_t^{inh} - R_t^0}{R_t^{inh}} \times 100 \quad [7]$$

with  $R_t^{inh}$  is the charge transfer resistance for the ODA treated samples and  $R_t^0$  is the charge transfer resistance for the samples without ODA.

For the magnetite and for the ODA treated magnetite at 80 °C (Table IV), the  $C_{dl}$  values were 200  $\mu\text{F cm}^{-2}$  and 24  $\mu\text{F cm}^{-2}$ , respectively. With magnetite only, the  $C_{dl}$  value is in the order of magnitude of a double layer capacitance ( $\approx 50 \mu\text{F cm}^{-2}$ ), slightly higher. This could be due to an increase of the surface area linked to the presence of the pores in the magnetite layer. For the ODA treated magnetite, the accessible surface area at the bottom of the through pores of the ODA film can be estimated from the ratio of the capacitances. A value of 12% was obtained. The calculated IE was equal to 87%, in good agreement with the capacitances ratio.

For the results at 120 °C (Table V) and 220 °C (Table VI), the  $C_{dl}$  values without ODA are of the same order of magnitude (200–300  $\mu\text{F cm}^{-2}$ ) as that obtained at 80 °C for the magnetite layer (Table IV). These results are in agreement with the formation of the magnetite layer during the exposure in the autoclave and once again confirms the good conductivity of the magnetite. With ODA, it is first important to note that the  $R_t$  values were determined with a significant margin of error. However, the  $R_t$  values are significantly higher than those obtained without ODA. Thus, the inhibitive efficiency reached very high level (IE > 99.9%). Secondly, it should be emphasized that the  $\alpha_{dl}$  values are low. This may be attributed to a porous electrode behaviour. As a consequence, the  $C_{dl}$  values cannot be accurately calculated. These results pointed out that the magnetite layers formed at 120 °C and 220 °C combined with the ODA molecules resulted in substantial improvement of the corrosion protection. Additional EIS experiments performed as a function of the exposure time in the  $\text{Na}_2\text{SO}_4$  solution (not shown) confirmed the beneficial role of the magnetite on the stability of the ODA film (the diagrams remained unchanged with immersion time). This confirmed the incorporation of the ODA molecules in the magnetite layer as suggested by the high resistivity values determined at the metal/film interface.

**Table IV.** Fitted parameter values obtained from the impedance diagram for the carbon steel covered by the magnetite and from the low-frequency time constant of the ODA treated magnetite.

	$R_e$ ( $\Omega \text{ cm}^2$ )	$R_t$ ( $\Omega \text{ cm}^2$ )	$Q_{dl}$ ( $\text{F cm}^{-2} \text{ s}^{(\alpha-1)}$ )	$\alpha$	$C_{dl}$ ( $\mu\text{F cm}^{-2}$ )	IE (%)	$\chi^2$
Magnetite	778	3200	$4.3 \times 10^{-4}$	0.63	200		0.21
Magnetite + ODA	1141	24600	$1.0 \times 10^{-4}$	0.60	24	87	0.38

Table V. Fitted parameter values obtained from the impedance diagram for the carbon steel sample treated at 120 °C during 168 h in the autoclave without ODA and from the low-frequency time constant of the ODA treated sample.

	$R_e$ ( $\Omega \text{ cm}^2$ )	$R_f$ ( $\Omega \text{ cm}^2$ )	$Q_{dl}$ ( $\text{F cm}^{-2} \text{ s}^{(\alpha-1)}$ )	$\alpha$	$C_{dl}$ ( $\mu\text{F cm}^{-2}$ )	IE (%)	$\chi^2$
Without	3661	16300	$3.0 \times 10^{-4}$	0.74	294		0.96
With ODA	3877	$3.5 \times 10^7$	$4.1 \times 10^{-6}$	0.48		99.95	0.72

Table VI. Fitted parameter values obtained from the impedance diagram for the carbon steel sample treated at 220 °C during 2 h in the autoclave without ODA and from the low-frequency time constant of the ODA treated sample.

	$R_e$ ( $\Omega \text{ cm}^2$ )	$R_f$ ( $\Omega \text{ cm}^2$ )	$Q_{dl}$ ( $\text{F cm}^{-2} \text{ s}^{(\alpha-1)}$ )	$\alpha$	$C_{dl}$ ( $\mu\text{F cm}^{-2}$ )	IE (%)	$\chi^2$
Without	4016	6300	$2.2 \times 10^{-4}$	0.70	169		0.41
With ODA	3930	$5 \times 10^7$	$2.8 \times 10^{-5}$	0.65		99.98	1.12

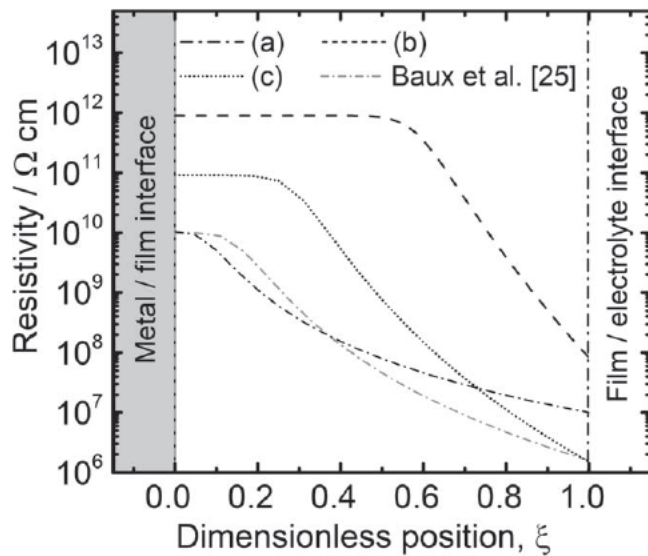


Figure 9. In depth resistivity profiles of the ODA layers as a function of position, calculated from Eq. 4, obtained from the impedance analysis (high frequency part): (a) on the synthetic magnetite (from Fig. 2) and comparison with the result obtained for the bare carbon steel with the same treatment<sup>25</sup>: 100 mg kg<sup>-1</sup> ODA; 80 °C; pH<sub>25</sub> °C = 10; 30 min, (b) after 168 h at 120 °C with 2 mg kg<sup>-1</sup> ODA (from Fig. 4) and (c) after 2 h at 220 °C with 25 mg kg<sup>-1</sup> ODA (from Figs. 5c and 5d).

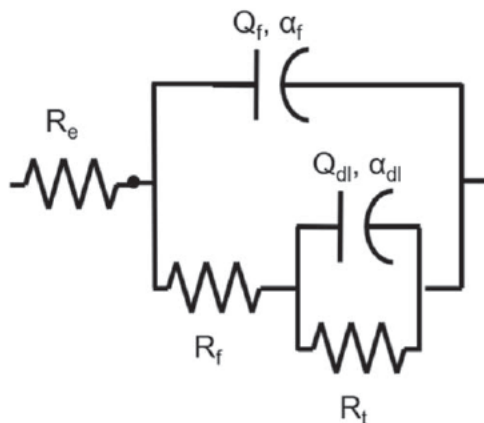




Figure 10. Electrical equivalent circuit used to fit the experimental diagrams when the presence of an ODA film was identified on the ODA treated samples.

## Conclusions

The ODA film formation was investigated in laboratory conditions, first on electrodeposited magnetite at 80 °C, and then in an autoclave at 120 °C, 220 °C and 275 °C. The presence of the ODA films on the carbon steel surface treated at 120 °C and at 220 °C was confirmed by surface observations and EIS measurements. For the carbon steel sample treated at 275 °C, the presence of an organic film was not shown. It was demonstrated that at 275 °C, ODA molecule degradation occurred and that more than 80 wt% disappeared in less than 6 h. From the impedance data analysis, the determined ODA films thickness was independent of the treatment conditions, and around 20 nm. However, the resistivity profiles, obtained from the power law model, were different according to the treatment conditions. At 120 °C and 220 °C, the impedance results accounted for the presence of a highly protective layer which would be efficient for long term protection of the carbon steel, attributed to the beneficial role of the magnetite formed during the exposure in the autoclave.

This study, based on a detailed analysis of the EIS measurements, provided a better understanding of the ODA behavior as a function of the temperature and shows that EIS is a powerful technique to characterize organic thin films on industrial samples.

## ORCID

Marion Roy  <https://orcid.org/0000-0003-3152-271X>  
Nadine Pèbère  <https://orcid.org/0000-0002-2728-0917>

## References

1. W. Hater, D. Olivet, and N. Rudschtzky, "The chemistry and properties of organic boiler feedwater additives based on film-forming amines and their use in steam generators." *Powerpl. Chem.*, **11**, 90 (2009).
2. C. W. Turner and L. Case, "Fouling of nuclear steam generators: fundamental studies, operating experience and remedial measures using chemical additives." *AECL Nucl. Rev.*, **2**, 61 (2013).
3. I. Betova, M. Bojinov, and T. Saario, "Film-forming amines in steam/water cycles —structure, properties, and influence on corrosion." *VTT., VTT-R-03234*, 1 (2014).
4. R. Crovetto, A. Rossi, D. Meskers, C. Pierce, J. Melzer, and K. Pearson, "State of knowledge on film-forming amines 2015." *EPRI, Palo Alto, CA, 2015*, 3002003678 (2015).
5. H.-H. Ge, G.-D. Zhou, Q.-Q. Liao, Y. G. Lee, and B. H. Loo, "A study of anti-corrosion behavior of octadecylamine-treated iron samples." *Appl. Surf. Sci.*, **156**, 39 (2000).
6. Q.-Q. Liao, G.-D. Zhou, H.-H. Ge, and L.-M. Qi, "Characterisation of surface film on iron samples treated with octadecylamine." *Corros. Eng. Sci. Technol.*, **42**, 102 (2007).
7. Q.-Q. Liao, H.-H. Ge, and G.-D. Zhou, "Use of octadecylamine for shutdown protection at power plants." *Mater. Perform.*, **47**, 58 (2008).
8. F. Mao, C. Dong, and D. D. Macdonald, "Effect of octadecylamine on the corrosion behavior of Type 316SS in acetate buffer." *Corros. Sci.*, **98**, 192 (2015).
9. M. Duprat, F. Moran, and F. Dabosi, "Some preliminary experiments regarding the corrosion inhibition of a carbon steel by oleylamino-propylene amine with tri (methyl-phosphonic) acid." *Corros. Sci.*, **23**, 1047 (1983).
10. P. Bommersbach, C. Alemany-Dumont, J. P. Millet, and B. Normand, "Formation and behaviour study of an environment-friendly corrosion inhibitor by electrochemical methods." *Electrochim. Acta*, **51**, 1076 (2005).



11. C.-E. Banica, E. Czempik, C. Vogt, and F. Schneider, "Influence of hot water conditioning on the corrosion behavior of carbon steel." *Mater. Corros.*, **53**, 256 (2002).
12. N. Ochoa, F. Moran, N. Pébère, and B. Tribollet, "Influence of flow on the corrosion inhibition of carbon steel by fatty amines in association with phosphonocarboxylic acid salts." *Corros. Sci.*, **47**, 593 (2005).
13. W. Kuang, J. A. Mathews, M. L. Taylor, and D. D. Macdonald, "The effect of Anodamine on the corrosion behavior of 1018 mild steel in deionized water: II. electrochemical impedance analysis." *Electrochim. Acta*, **136**, 493 (2014).
14. E. Pensini, R. Van Lier, F. Cuoq, W. Hater, and T. Halthur, "Enhanced corrosion resistance of metal surfaces by film forming amines: a comparative study between cyclohexanamine and 2-(diethylamino)ethanol based formulations." *Water Resources and Industry*, **20**, 93 (2018).
15. R. D. Braun, E. E. Lopez, and D. Vollmer, "Low molecular weight straight-chain amines as corrosion inhibitors." *Corros. Sci.*, **34**, 1251 (1993).
16. E. C. Roberto, A. de Oliveira Wanderley Neto, C. A. Martínez-Huitle, J. L. Cardozo Fonseca, T. N. de Castro Dantas, and A. Gurgel, "The effect of type of self-assembled system and pH on the efficiency of corrosion inhibition of carbon steel surfaces." *Prog. Org. Coat.*, **76**, 1308 (2013).
17. E. V. Chernyshev, E. N. Veprov, V. A. Petrov, S. L. Bogdanov, T. Y. Levina, T. I. Petrova, V. I. Kashinskii, A. A. Zonov, and A. E. Verkhovskii, "Increasing the corrosion resistance of equipment due to the use of film-forming amines." *Power Technol. Eng.*, **40**, 34 (2006).
18. S. A. Cao, J. Y. Hu, J. L. Xie, Q. Q. Liang, and L. Yin, "Research on the film-forming characteristics of octadecylamine at high temperatures." *Anti-Corrosion Methods Mater.*, **60**, 14 (2013).
19. A. V. Kurshakov, A. V. Ryzhenkov, A. A. Bodrov, O. V. Ryzhenkov, A. A. Patakin, and E. F. Chernov, "Heat transfer enhancement in steam-turbine condensers with the use of surface-active substances." *Therm. Eng.*, **61**, 785 (2014).
20. B. M. Fan, G. Wei, Z. Zhang, and N. Qiao, "Characterization of a supramolecular complex based on octadecylamine and  $\beta$ -cyclodextrin and its corrosion inhibition properties in condensate water." *Corros. Sci.*, **83**, 75 (2014).
21. B. M. Fan, Y. Ma, M. Wang, H. Hao, B. Yang, J. Lv, and H. Sun, "Revealing the assembly mechanism of an octadecylamine based supramolecular complex on mild steel in condensate water: Correlative experimental and theoretical studies." *J. Mol. Liquids*, **292**, 111446 (2019).
22. K. Sipilä and T. Saario, "Effect of octadecylamine on carbon steel corrosion under PWR secondary side conditions." *VTT, VTT-R-06077* (2014).
23. E. Jäppinen, T. Ikäläinen, S. Järvinmäki, T. Saario, K. Sipilä, and M. Bojinov, "Corrosion behavior of carbon steel coated with octadecylamine in the secondary circuit of a pressurized water reactor." *J. Materials Eng. Perform.*, **26**, 6037 (2017).
24. B. N. Khodyrev, A. L. Krichevtsov, and A. A. Sokolyuk, "Studying the processes relating to oxidation of organic substances contained in the coolant of thermal and nuclear power stations." *Therm. Eng.*, **57**, 553 (2010).
25. J. Baux, N. Caussé, J. Esvan, S. Delaunay, J. Tireau, M. Roy, D. You, and N. Pébère, "Impedance analysis of film-forming amines for the corrosion protection of a carbon steel." *Electrochim. Acta*, **283**, 699 (2018).
26. J. E. Castle and G. M. W. Mann, "The mechanism of a porous oxide film on steel." *Corros. Sci.*, **6**, 253 (1966).
27. J. H. Ashford, R. Garnsey, and G. M. W. Mann, "Corrosion of mild steel under heat transfer in high temperature aerated sodium chloride solutions." *Corros. Sci.*, **6**, 515 (1974).
28. C. Goujon, T. Pauporté, C. Mansour, S. Delaunay, and J. Bretelle, "Electrochemical deposition of thick iron oxide films on nickel based superalloy substrates." *Electrochim. Acta*, **176**, 230 (2015).
29. C. Wood and R. J. M. Konings, "Water Chemistry Control in LWRs." *Comprehensive Nuclear Materials* (Elsevier, Amsterdam) **17** (2012).
30. P. Tremaine and J. Leblanc, "The solubility of magnetite and the hydrolysis and oxidation of  $Fe^{2+}$  in water to 300 °C." *J. Sol. Chem.*, **9**, 415 (1980).
31. D. Lister and S. Uchida, "Determining water chemistry conditions in nuclear reactor coolants." *J. Nuclear Sci. Technol.*, **52**, 451 (2015).
32. M. E. Orazem, N. Pébère, and B. Tribollet, "Enhanced graphical representation of electrochemical impedance data." *J. Electrochem. Soc.*, **153**, B129 (2006).
33. M. Benoit, C. Bataillon, B. Gwinner, F. Miserque, M. E. Orazem, C. M. Sánchez-sánchez, B. Tribollet, and V. Vivier, "Comparison of different methods for measuring the passive film thickness on metals." *Electrochim. Acta*, **201**, 340 (2016).
34. A. S. Nguyen, N. Causse, M. Musiani, M. E. Orazem, N. Pébère, B. Tribollet, and V. Vivier, "Determination of water uptake in organic coatings deposited on 2024 aluminium alloy: Comparison between impedance measurements and gravimetry." *Prog. Org. Coatings*, **112**, 93 (2017).
35. S. Chakri, I. Frateur, M. E. Orazem, E. M. M. Sutter, T. T. M. Tran, B. Tribollet, and V. Vivier, "Improved EIS analysis of the electrochemical behaviour of carbon steel in alkaline solution." *Electrochim. Acta*, **246**, 924 (2017).
36. D. R. Lide, *CRC Handbook of Chemistry and Physics* (CRC Press, United States of America) 84th ed. (2003).
37. B. Hirschorn, M. E. Orazem, B. Tribollet, V. Vivier, I. Frateur, and M. Musiani, "Constant-phase-element behavior caused by resistivity distributions in films. I: theory." *J. Electrochem. Soc.*, **157**, C452 (2010).
38. B. Hirschorn, M. E. Orazem, B. Tribollet, V. Vivier, I. Frateur, and M. Musiani, "Constant-phase-element behavior caused by resistivity distributions in films. II: applications." *J. Electrochem. Soc.*, **157**, C458 (2010).
39. I. Frateur, C. Deslouis, M. Orazem, and B. Tribollet, "Modeling of the cast iron/drinking water system by electrochemical impedance spectroscopy." *Electrochim. Acta*, **44**, 4345 (1999).
40. G. J. Brug, A. L. G. van den Eeden, M. Sluyters-Rehbach, and J. H. Sluyters, "The analysis of electrode impedances complicated by the presence of a constant phase element." *J. Electroanal. Chem.*, **176**, 275 (1984).